JOURNAL OF SYNCHROTRON RADIATION

ISSN 1600-5775

Local structure change of luminescent Ag zeolite-A and -X studied by *in situ* XAFS and IR spectroscopy

Takafumi Miyanaga,* Yushi Suzuki, Sho Narita and Reki Nakamura

Department of Mathematics and Physics, Hirosaki University, 3 Bunkyo-cho, Hirosaki, Aomori 036-856, Japan. *Correspondence e-mail: takaf@hirosaki-u.ac.jp

Received 17 April 2020
Accepted 14 September 2020

Edited by S. M. Heald, Argonne National Laboratory, USA

Keywords: XAFS; zeolites; photoluminescence; IR.

The *in situ* X-ray absorption fine structure (XAFS) for the structural changes of Ag clusters produced in the cavity of luminescent zeolites by thermal treatment of Ag zeolite-A and Ag zeolite-X has been studied. The following procedures are compared: (i) samples are heated and cooled to room temperature under atmosphere (under air); (ii) samples are heated and cooled to room temperature in a vacuum and then exposed to air. It was confirmed that the Ag clusters were broken when the Ag zeolite was exposed to air for Ag zeolite-X, which complements our previous results for Ag_{12}-A. It is suggested that the deformation of the Ag clusters plays an important role in the generation of a strong photoluminescence band, and Ag clusters may not be direct species producing the strong photoluminescence. The local structure of the Ag ions was found to be slightly different from that of the unheated species. The difference may originate from the formation and breakdown of Ag clusters in the zeolite cavity.

1. Introdution

Zeolites show unique properties owing to the cavities and cages existing in the crystalline aluminosilicates. Several types of cations can be easily exchanged with Na^+ ions in the Na-type zeolites and their unique physical and chemical properties will depend on the substituted cations (Kim *et al.*, 2003).

Ag zeolites are typical functional materials, and can be used in information storage, catalysis, pressure and chemical sensors, and anti-bacterial materials. In the field of nanoscale science, the importance of metal nanoparticles and nanoclusters increases. Nanoparticles and clusters are produced simply in the zeolite cavity, and their particle sizes can be well controlled (Kim & Seff, 1987; Sun & Seff, 1994; Seifert *et al.*, 2000; Calzaferri *et al.*, 2003).

It has been reported that Ag-type zeolite-A, when cooled to room temperature and mixed with air after being heated at 500°C for 24 h under vacuum, shows a strong photoluminescence (PL) band around 2.18 eV (Hoshino *et al.*, 2008). The same behaviour can be observed in the atmosphere. The intensity of the PL band is known to be affected by the conditions of the heating steps and the types of atmospheric gases exposed to after cooling (Nakamura *et al.*, 2014). However, the detailed mechanism of the PL has been unclear. On the other hand, when the Ag-type zeolite is heated, the lattice water molecules in the cavity are removed and the Ag^+ ion is reduced to Ag^0; 'Ag clusters' are produced inside the zeolite (Hoshino *et al.*, 2008).

Recently the relation between Ag oligomers and PL was studied (De Cremer *et al.*, 2009, 2010; Coutino-Gonzalez *et al.*, 2013). The degree of Ag loading in the framework and the

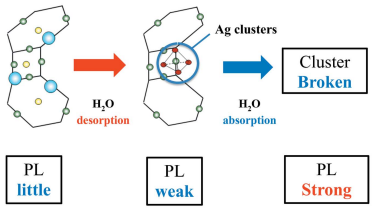

type of framework (A, X and Y) can tune the ionization potential, which correlates with the optical properties.

X-ray absorption fine structure (XAFS) is a powerful tool for studying the local structure in nanoscale materials and is suitable for *in situ* measurements (Hoshino *et al.*, 2008; Nakamura *et al.*, 2014; Altantzis *et al.*, 2016). So far it has been reported that Ag_4 clusters are observed as the origin of the green/yellow emission in Ag zeolite-A and of the yellow emission in Ag zeolite-X (Altantzis *et al.*, 2016; Fenwick *et al.*, 2016); and Ag_3 clusters are observed as the origin of the green emission in Ag zeolite-Y (Coutino-Gonzalez *et al.*, 2015).

In a previous paper (Nakamura *et al.*, 2014) we investigated by XAFS the relation between the existence of Ag clusters and the enhancement of the PL intensity in order to clarify the PL mechanisms for Ag zeolite-A. We carried out *in situ* XAFS measurements under the same conditions as the PL measurements, and attempted to expose the zeolites to various gases – oxygen, nitrogen, water vapour and their mixtures – after heating, in order to study the origin of the structural change of the Ag clusters. The result indicates that the Ag clusters produced by heating are destroyed by the introduction of air or a gas mixture of H_2O and N_2, but the Ag clusters remain intact when O_2 or N_2 are introduced. Coutino-Gonzalez *et al.* reported that the X-ray beam has a great influence on the dynamics of formation and destruction of luminescent Ag clusters in zeolites (Coutino-Gonzalez *et al.*, 2014), but our result for the introduction of O_2 and N_2 gas is contradicted. We suppose that the existence of H_2O and N_2 gas is important for the destruction of Ag clusters and the effect of X-rays is not essential for cluster destruction.

In this paper, we further investigate how Ag clusters are destroyed after exposure to air in Ag zeolite-A and -X from XAFS and discuss the mechanism of PL in Ag-zeolites. Two procedures were applied: (i) Ag-zeolites are heated at a certain temperature in the atmosphere and cooled in air (including H_2O and N_2); (ii) Ag-zeolites are heated under vacuum and cooled to room temperature (RT) and then exposed to air.

2. Experimental

2.1. Sample preparation

Fully Ag^+-exchanged zeolite A (hydrated 12Ag-A) powder samples were prepared by immersing the hydrated 12Na-A in 0.1 *M* $AgNO_3$ solution for 24 h at 25°C. After careful filtration the 12Ag-A powder was dried under air at RT in a darkroom. The sample is called 'Ag_{12}-A' in this paper. Analogously, the fully Ag^+-exchanged zeolite X (hydrated 86Ag-X) and zeolite Y (51.2Ag-Y) were prepared by a similar procedure and named 'Ag_{86}-X' and '$Ag_{51.2}$-Y', respectively. Detailed sample preparation procedures are reported in previous papers (Hoshino *et al.*, 2008; Miyanaga *et al.*, 2013).

Ag_{12}-A, Ag_{86}-X and $Ag_{51.2}$-Y were heated at 400 or 500°C in atmosphere or in vacuum to produce the Ag clusters. After keeping at 400 or 500°C for 24 h, they were cooled to RT in the atmosphere. In the vacuum process the sample was exposed to air after cooling to RT. *In situ* XAFS measurements were performed for each process.

2.2. PL measurements

PL spectra were obtained using a UV-VIS spectrometer (SPM-002; KLV) where a 405 nm violet laser (SU-61-405; audio-technica) and 365 nm LED (Ocean Optics LLS-LED365) were used for excitation. A high-vacuum chamber (RVX-3) was used to measure the PL spectra under various atmospheric conditions. PL was obtained after 24 h exposure to air.

2.3. XAFS measurements and data analysis

X-ray absorption spectra of the Ag *K*-edge (25.5 keV) were measured in transmission mode at beamline NW10A at Photon Factory, KEK, Japan. A Si(311) monochromator was used. For *in situ* XAFS measurements the RVX-3 vacuum chamber was used (Miyanaga *et al.*, 2016). The powder sample was mounted on the sample cell in the RVX-3 chamber, in which temperature can be controlled from RT to 500°C and pressure can be controlled by vacuum pump ($\sim 10^{-5}$ Pa). In order to discuss quantitatively the change of local structure around Ag, we performed non-linear least-squares fitting (curve-fitting) to EXAFS spectra using the equation

$$\chi(k) = \sum_j \frac{S_0^2 N_j}{k r_j^2} f_j(k, r_j) \exp\left(-2\sigma_j^2 k^2\right) \times \exp\left[-2r_j/\lambda(k)\right] \sin\left[2kr_j + \phi_j(k)\right], \quad (1)$$

where r_j is the interatomic distance between X-ray absorbing Ag and photoelectron scattering atoms in the jth shell, and N_j is the coordination number of the jth shell. $f_j(k,r_j)$ and $\varphi_j(k)$ are the backscattering amplitude and phase shift functions, respectively, which were calculated using the *FEFF8.10* code (Ankudinov *et al.*, 1998). The k-range in the curve-fitting method is from ~3.0 to 9.0 Å^{-1} for the Ag *K*-edge. The fits were performed in k-space to the $k^2\chi(k)$ function after back-transforming the *R*-space Fourier transform with the Hamming window. $\lambda(k)$ is the photoelectron mean free path obtained by *FEFF 8.10* calculation (Ankudinov *et al.*, 1998). Ag foil and $AgNO_3$ were used as standard samples and S_0^2 (reduction factor by many-body effect) was determined as 0.83. As the origin of the photoelectron kinetic energy, E_0, in the fits we used the single value of 4.3 eV as the energy shift from the absorption edge.

As will be discussed later, we applied three-shell fitting for the EXAFS data. The number of unknown parameters was nine (r, N and σ for each shell). On the other hand, the number of possible fitting parameters was ten, obtained from the refinement of XAFS standards and criteria.

The EXAFS oscillation function was extracted from the X-ray absorption spectra and Fourier transformed using the *XANADU* code (Sakane *et al.*, 1993). In order to obtain the structural parameters, the EXAFS function was fitted in k-space by a non-linear least-squares method using the theore-

tical parameters calculated by *FEFF 8.10* (Ankudinov *et al.*, 1998).

3. Results

3.1. Photoluminescence of Ag_{12}-A, Ag_{86}-X and $Ag_{51.2}$-Y

First, we present the results of the PL measurements. Fig. 1 shows the PL curves for luminescent species of Ag_{12}-A, Ag_{86}-X and $Ag_{51.2}$-Y, which were cooled to RT after heating to 400 or 500°C. Ag_{12}-A and Ag_{86}-X show a strong PL band at 2.18 eV and an intermediate band at 2.24 eV, respectively, after excitation by the 405 nm laser (*a*). On the other hand, a strong PL band was observed at 2.40 eV for $Ag_{51.2}$-Y after 365 nm excitation in addition to the 2.18 eV and 2.24 eV bands for Ag_{12}-A and Ag_{86}-X (*b*).

3.2. XAFS for Ag_{12}-A under atmosphere

In this subsection, we present the EXAFS results for Ag_{12}-A heated to 500°C, kept for 24 h and then cooled to RT under atmospheric conditions. Fig. 2 shows the Ag-*K* X-ray absorption near-edge structure (XANES) (*a*), $k^2\chi(k)$ spectra (*b*) and its Fourier transform (FT) (*c*) for Ag_{12}-A unheated at RT in the atmosphere (black line), heated at 500°C (red line), and cooled to RT after heating to 500°C (blue line). After the heating, the intensity of the white peak in the XANES becomes smaller and the energy shifts to slightly higher. After exposure to air at RT the XANES returns to that of the unheated species. It is found that the structure around 3.5 $Å^{-1}$ in (*b*) shows a clear change at 500°C, which is the characteristic feature of Ag clusters formation (Hoshino *et al.*, 2008). In Fig. 2(*c*), the first FT peak around 1.8 Å is assigned to Ag—O_1 (nearest neighbour oxygen from the zeolite framework and lattice water molecule in the cage). The second FT peak around 2.8 Å includes the contribution from Ag—Ag and Ag—O_2 (further next nearest oxygen atom in the zeolite framework). The intensity of the FT peaks measured at 500°C is smaller than that measured at RT because of the large Debye–Waller factor. The fact that the $k^2\chi(k)$ spectra for the sample cooled to RT after heating to 500°C are almost the same as the unheated one indicates that the Ag clusters produced in the process of heating to 500°C were broken by

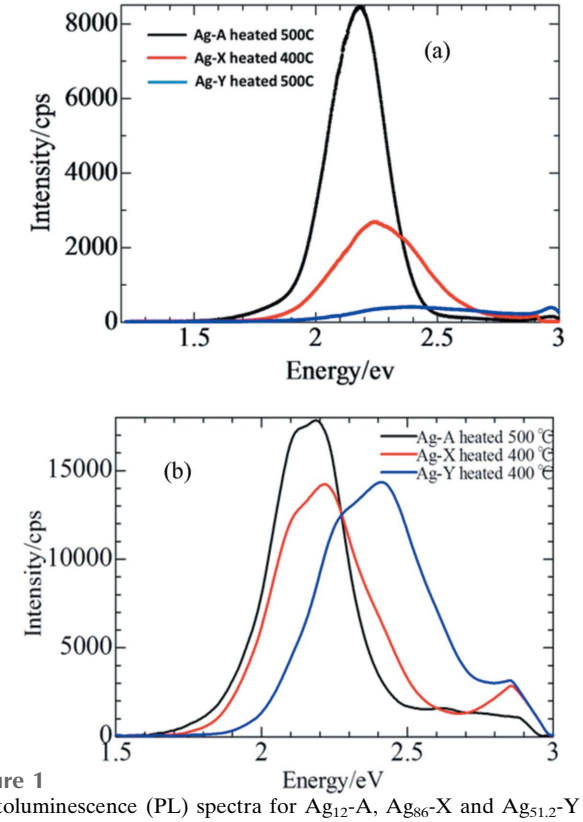

Figure 1
Photoluminescence (PL) spectra for Ag_{12}-A, Ag_{86}-X and $Ag_{51.2}$-Y after heating under atmosphere after excitation by (*a*) 405 nm laser and (*b*) 365 nm LED. The relative intensities between (*a*) and (*b*) are not comparable.

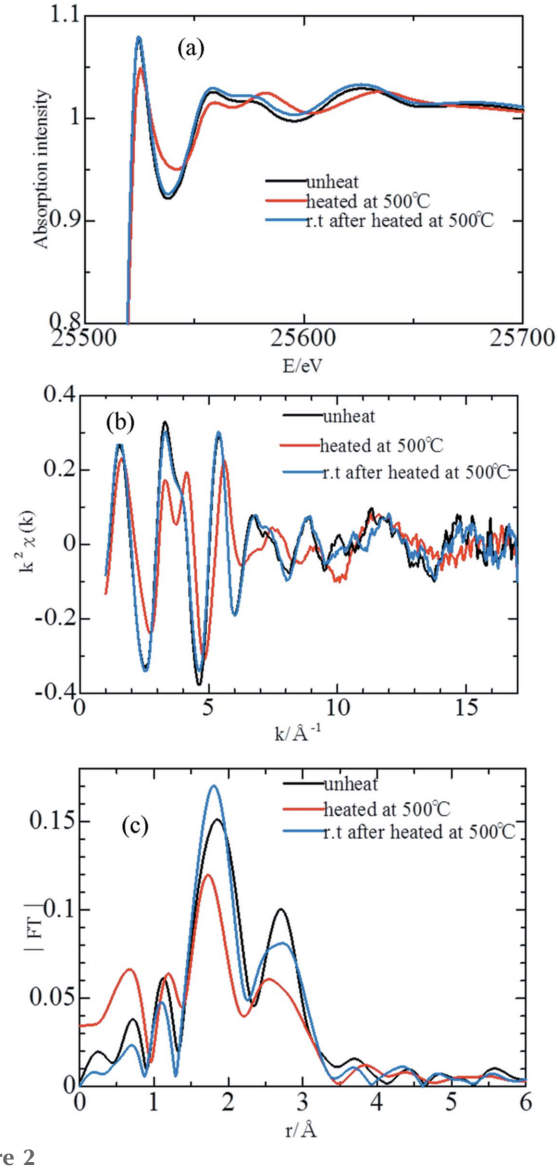

Figure 2
Ag-*K* (*a*) XANES spectra, (*b*) $k^2\chi(k)$ spectra and (*c*) Fourier transform for Ag_{12}-A unheated at RT in atmosphere (black line), heated for 24 h and measured at 500°C (red line), and cooled to RT after heating to 500°C (blue line).

Table 1
Structural parameters r, N and σ for Ag_{12}-A for the process that heated under atmosphere.

	r_{O1} (Å)	N_{O1}	σ_{O1} (Å)	r_{O2} (Å)	N_{O2}	σ_{O2} (Å)	r_{Ag} (Å)	N_{Ag}	σ_{Ag} (Å)
Unheated sample measured at RT	2.38	3.7	0.13	2.87	0.9	0.10	2.87	1.3	0.11
Heated at 500°C for 24 h	2.28	3.3	0.15	2.70	1.7	0.16	2.81	3.1	0.17
Cooled to RT after heating in air	2.37	3.4	0.13	2.82	1.1	0.10	2.87	1.2	0.11

mixing with air, as discussed previously (Nakamura *et al.*, 2014). On the other hand, their FT spectra are slightly different and a detailed discussion will be given later.

Table 1 shows the structural parameters r and N for O_1, O_2 and Ag for Ag_{12}-A for the process of heating under atmospheric conditions. During the heating process, r_{O1} decreases from 2.38 Å to 2.28 Å and N_{O1} is also reduced from 3.7 to 3.3, indicating the removal of lattice water molecules in the cavity. Even in the unheated species, a small portion of the Ag—Ag pair exists in the cavity naturally (r_{Ag} = 2.87 ± 0.01 Å and N_{Ag} = 1.3 ± 0.3). In the heating process, N_{Ag} increases from 1.3 ± 0.3 to 3.1 ± 0.3 which means that the formation of Ag clusters and the size of the clusters is almost the same as for the Ag_4 cluster, as previously reported (Fenwick *et al.*, 2016). At this stage, Ag_{12}-A does not show a strong PL yet.

In the final process of cooling to RT after heating to 500°C, water molecules are incorporated into the cavity again. The parameters are almost the same as for the unheated case: for example, N_{O1} (3.4 ± 0.3) and N_{Ag} (1.2 ± 0.3) are almost the same as for the unheated N_{O1} (3.7 ± 0.3) and N_{Ag} (1.3 ± 0.3).

3.3. XAFS for Ag_{12}-A under vacuum

Next, we discuss the case where Ag_{12}-A was heated under vacuum and air was introduced after cooling to RT. Fig. 3 shows the Ag-*K* XANES (*a*), $k^2\chi(k)$ spectra (*b*) and its FT (*c*) for Ag_{12}-A unheated species measured at RT in atmosphere (black line), unheated under vacuum (blue line), heated at 500°C (red line) for 24 h, and cooled to RT in vacuum (green line). After the heating, the intensity of the white peak in the XANES becomes smaller and the energy shifts to slightly higher. The behaviour is almost the same as that under atmosphere. As discussed in the previous subsection, the characteristic structure around 3.5 $Å^{-1}$ shows the existence of Ag clusters under vacuum state, see Fig. 3(*b*). In Fig. 3(*c*), a clear contribution from Ag—Ag contact can be seen in the vacuum condition and the Ag—Ag contribution increases with heating.

Table 2 shows the structural parameters for Ag_{12}-A after heating in vacuum and 12 h after air introduction. During the first evacuation process, a part of a water molecule is removed from the cavity and the Ag cluster is grown. After continuous heating to 500°C, the Ag clustering process proceeds. However, N_{Ag} (= 2.8 ± 0.3) is slightly smaller than for the process in air discussed in the previous subsection (N_{Ag} = 3.1 ± 0.3) but the reason for this is still unclear. The structural parameters after 12 h of air exposure are almost the same as the result for cooling to RT in air as in the previous subsection (Table 1).

3.4. XAFS for Ag_{86}-X under atmosphere

In this subsection we discuss the result for Ag_{86}-X under atmosphere. Fig. 4 shows the Ag-*K* XANES (*a*), $k^2\chi(k)$ spectra (*b*) and its FT (*c*) for Ag_{86}-X unheated at RT in atmosphere (black line), heated at 400°C (red line), and cooled to RT after heating to 500°C (blue line). After the

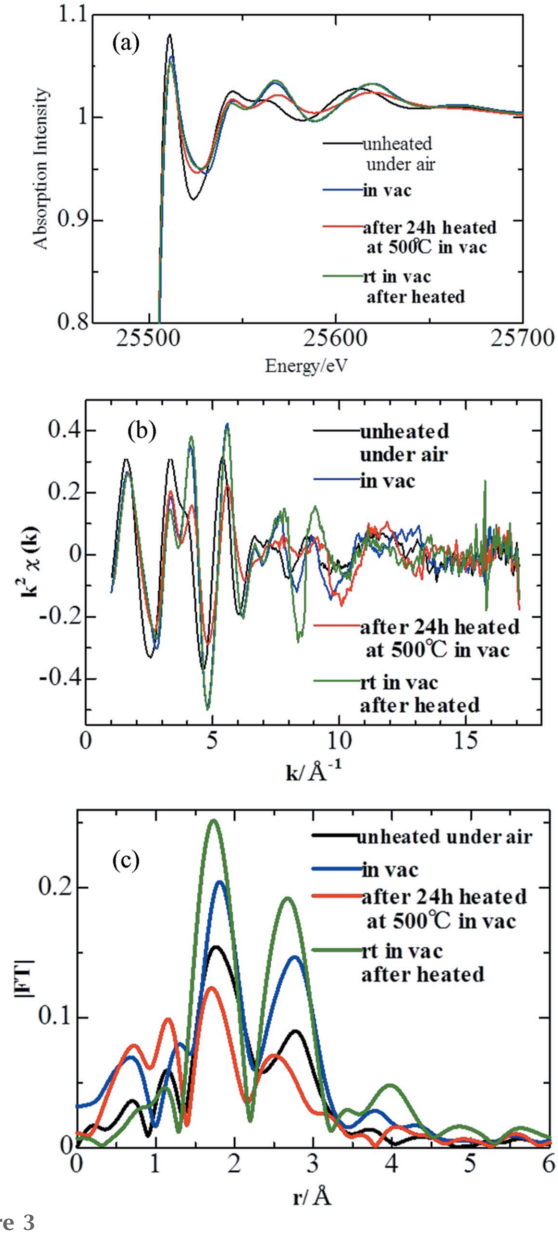

Figure 3
Ag-*K* (*a*) XANES spectra, (*b*) $k^2\chi(k)$ spectra and (*c*) Fourier transform for Ag_{12}-A unheated species measured at RT in atmosphere (black line), unheated under vacuum (blue line), heated at 500°C for 24 h (red line), and cooled to RT in vacuum (green line).

Table 2
Structural parameters r, N and σ for Ag_{12}-A for the process that heated in vacuum and 12 h after air introduction.

	r_{O1} (Å)	N_{O1}	σ_{O1} (Å)	r_{O2} (Å)	N_{O2}	σ_{O2} (Å)	r_{Ag} (Å)	N_{Ag}	σ_{Ag} (Å)
Vacuum at RT	2.29	3.2	0.13	2.82	1.7	0.10	2.83	2.0	0.11
After 24 h in vacuum at 500°C	2.28	2.9	0.14	2.71	2.1	0.16	2.80	2.8	0.17
RT in vacuum after heating	2.27	3.4	0.13	2.82	1.4	0.12	2.81	2.6	0.11
Exposure to air for 12 h	2.37	3.2	0.13	2.88	1.0	0.10	2.86	1.3	0.11

Table 3
Structural parameters r, N and σ for Ag_{86}-X for the process that heated under atmosphere.

	r_{O1} (Å)	N_{O1}	σ_{O1} (Å)	r_{O2} (Å)	N_{O2}	σ_{O2} (Å)	r_{Ag} (Å)	N_{Ag}	σ_{Ag} (Å)
Unheated sample measured at RT	2.38	3.8	0.14	3.06	0.7	0.08	2.98	1.7	0.15
Heated at 400°C for 24 h	2.28	3.1	0.16	2.71	1.0	0.17	2.84	2.3	0.20
Cooled to RT after heating in air	2.37	3.5	0.14	3.05	0.6	0.08	2.98	1.5	0.15

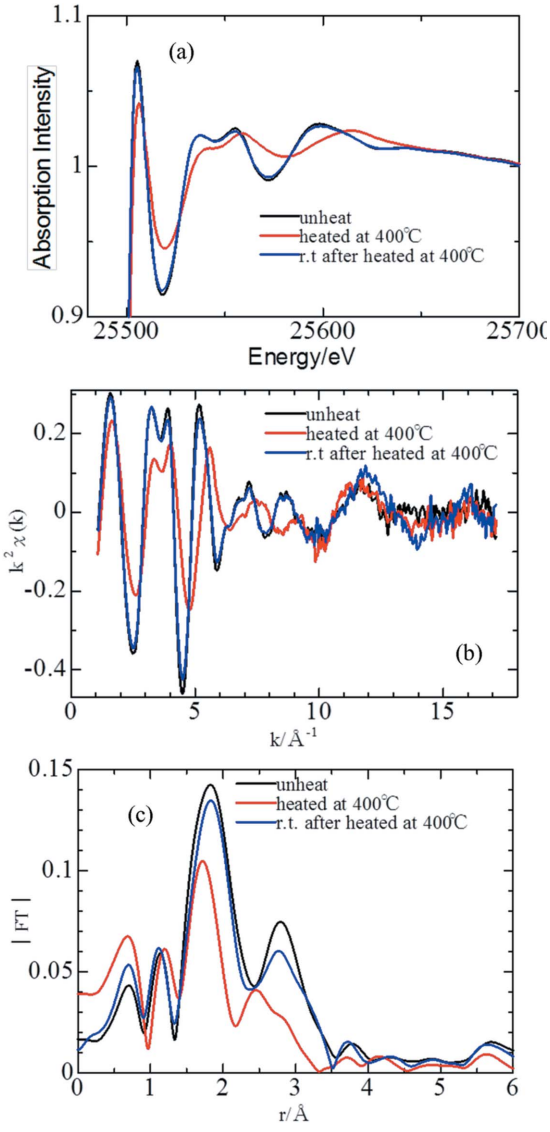

Figure 4
Ag-K (a) XANES spectra, (b) $k^2\chi(k)$ spectra and (c) Fourier transform for Ag_{86}-X unheated at RT in atmosphere (black line), heated for 24 h and measured at 400°C (red line), and cooled to RT after heating to 400°C (blue line).

heating, the intensity of the white peak in the XANES becomes smaller and the energy shifts to slightly higher value. After air exposure at RT the XANES returns to that of the unheated species. In the case of zeolite-X, there is a characteristic feature around 3.5 $Å^{-1}$ even in the unheated state in (b) and it becomes prominent after heating to 400°C. In (c) peaks for the heated to 400°C sample shift to shorter than unheated and after heated sample. Both spectra for (a) and (b) for the cooled to RT sample are almost the same as for the unheated one but slightly different as discussed for Ag zeolite-A.

Table 3 shows structural parameters for Ag_{86}-X for the process that heated under atmosphere. The structural change of r_{O1} is almost the same as that for Ag_{12}-A. On the other hand, r_{O2} and r_{Ag} are different; both are longer than for Ag_{12}-A. N_{Ag} for Ag_{86}-X is smaller than that for Ag_{12}-A.

Values of r_{Ag} for the unheated sample and clusters are 2.98 ± 0.01 Å and 2.84 ± 0.01 Å, longer than for Ag_{12}-A (2.87 ± 0.01 Å and 2.81 ± 0.01 Å). Ag atoms are strongly connected to O atoms in the framework; however, r_{O1} is similar to that for Ag_{12}-A. The cavity size for zeolite-X is larger than that for zeolite-A; then r_{Ag} of the Ag clusters is longer than that for Ag_{12}-A.

3.5. XAFS for Ag_{86}-X under vacuum

Fig. 5 shows the Ag-K XANES (a), $k^2\chi(k)$ spectra (b) and its FT (c) for Ag_{86}-X unheated at RT in atmosphere (black line), RT in vacuum (red line), heated for 24 h and measured at 400°C (yellow line), cooled to RT after heating to 400°C (blue line), and after 8 h exposure to air (green line). The qualitative change of structure is the same as for that under atmospheric conditions. After the heating, the intensity of the white peak in the XANES becomes smaller and the energy shifts to slightly higher. After air exposure at RT the XANES returns to that of the unheated species. It is noted that the change in XANES for Ag_{86}-X under vacuum is smaller than for other systems.

Table 4 shows the structural parameters for Ag_{86}-X for the process that heated under vacuum and 8 h after air introduction. N_{Ag} (= 2.8 ± 0.3) is larger than that for atmospheric

Table 4
Structural parameters r, N and σ for Ag_{86}-X for the process that heated in vacuum and 12 h after air introduction.

	r_{O1} (Å)	N_{O1}	σ_{O1} (Å)	r_{O2} (Å)	N_{O2}	σ_{O2} (Å)	r_{Ag} (Å)	N_{Ag}	σ_{Ag} (Å)
Vacuum at RT	2.29	3.4	0.14	2.94	0.4	0.10	2.84	2.1	0.15
After 24 h in vacuum at 500°C	2.29	3.2	0.15	2.73	3.0	0.18	2.82	2.8	0.18
RT in vacuum after heating	2.29	2.5	0.12	2.84	1.4	0.15	2.82	1.9	0.12
Exposure to air for 8 h	2.37	3.3	0.14	3.02	0.5	0.08	2.96	1.5	0.15

conditions in the previous subsection ($N_{Ag} = 2.3 \pm 0.3$). This cluster size ($N_{Ag} = 2.8 \pm 0.3$) corresponds to 'Cluster Type I' discussed in our previous paper (Miyanaga *et al.*, 2013) for Ag_{86}-X, where the cluster size depends on the filling rate of Ag ions in the zeolite-X cavity. On the other hand, the result for this cluster size ($N_{Ag} = 2.8 \pm 0.3$) corresponds to that for the Ag_4 cluster as proposed by Altantzis *et al.* (2016) and Fenwick *et al.* (2016). From the coordination number, it is not so easy to determine which cluster model, Ag_4 or Ag_8, is adequate.

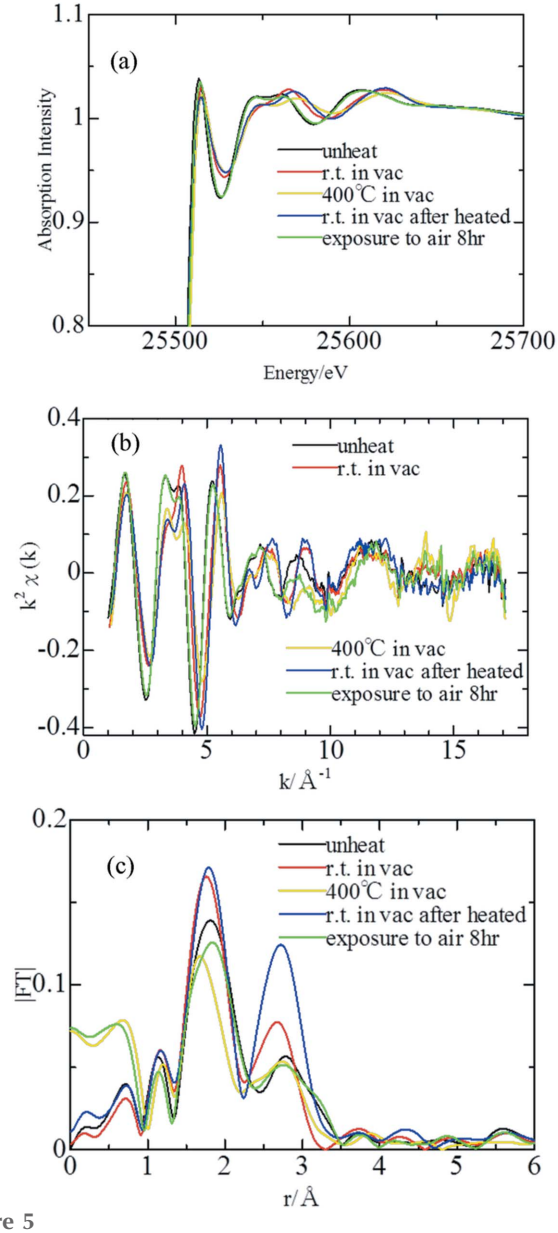

Figure 5
Ag-*K* (*a*) XANES spectra, (*b*) $k^2\chi(k)$ spectra and (*c*) Fourier transform for Ag_{86}-X unheated at RT in atmosphere (black line), RT in vacuum (red line), heated for 24 h and measured at 400°C (yellow line), cooled to RT after heating to 400°C (blue line), and after 8 h exposure to air (green line).

3.6. IR spectra of Ag_{12}-A

Fig. 6 shows the infrared (IR) transmission spectra of Ag_{12}-A for the sample exposed to air (*a*) and oxygen (*b*). The black line is for the unheated Ag zeolite. Due to the complicated structure of zeolite, the bands are superimposed on the various Si—O and Al—O contributions, so it is extremely difficult to distinguish between them. Only the assignment of the absorption band around the 1000 cm^{-1} region as $\nu(T—O)$ (T = Si or Al) (Rodrigues, 1995) is possible. IR bands at relatively higher wavenumber are assigned to the ν_{as} (asymmetric) mode, and the lower region to the ν_s (symmetric) mode. A bending mode should appear in the lower energy region but is not shown here. The green line shows the spectrum of Ag_{12}-A cooled to RT after heating for 24 h at 500°C in vacuum (measured in a vacuum). Compared with the

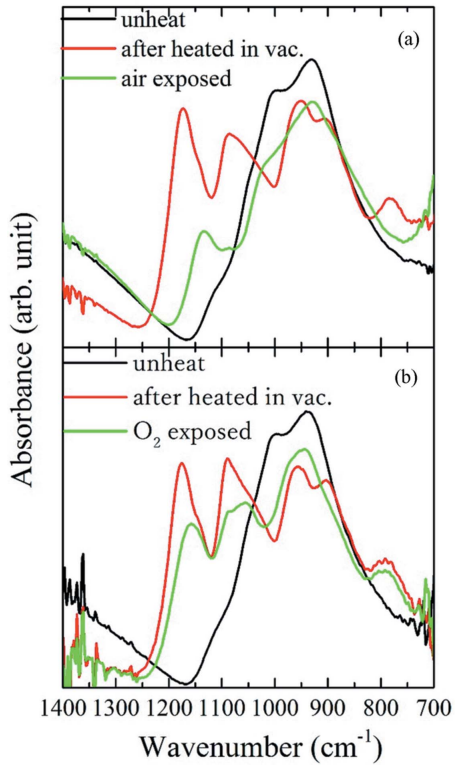

Figure 6
IR spectra of Ag_{12}-A for (*a*) air exposure and (*b*) oxygen exposure.

unheated case, the absorption band has changed drastically. While the individual band assignment is not possible as mentioned above, by considering the results of XAFS it is reasonable to assume that the change is due to the formation of Ag clusters. For cluster formation, it is necessary that Ag^+ ions (at least partially) are reduced to Ag^0; also Ag which is to be aggregated away from the site of the Ag^+ ion was located. This reduction of the ions and change of position also affects the vibrations of the framework in each case. The changes in the distances between the framework and the Ag atoms and the changes in the electrostatic attraction of Ag^+ can perturb the vibration of the T—O bond. In other words, it can be said that the IR is sensitive to such a change in the zeolite framework. The green lines in Fig. 6 are the spectra for the case of introducing air (*a*) and oxygen (*b*) into the zeolite, which are cooled to RT after the vacuum heating. After introduction of the air, the spectrum greatly changed again, and is much closer to that of the unheated spectrum (black line). Whereas for XAFS the air intake after heating substantially coincides with that for the unheated one, IR spectra for both states are not completely the same as each other. A distinct band appeared at 1140 cm^{-1} and the strength of the main band at 1000–900 cm^{-1} decreased slightly. After the introduction of oxygen, the situation is different. The structures at 1100 cm^{-1} and 1180 cm^{-1} still remain after the introduction of O_2 gas, indicating that Ag clusters are not destroyed by O_2 gas. This supports our previous XAFS results (Nakamura *et al.*, 2014).

4. Discussion

In this section we discuss the above results for Ag_{12}-A and Ag_{86}-X. As already discussed in the previous paper for Ag_{12}-A (Hoshino *et al.*, 2008; Nakamura *et al.*, 2014), Ag clusters are produced in the zeolite cavity by heating in air or in vacuum, and the qualitative results are the same for Ag_{86}-X. For Ag_{12}-A, the Ag cluster is grown only by evacuating the sample at RT. On the other hand, for Ag_{86}-X, the formation of Ag clusters is incomplete by only evacuating the sample at RT, but is completed by heating to ∼400°C.

The formation of Ag clusters in the zeolite cavity is confirmed by the increase of the coordination number of Ag—Ag (N_{Ag}) from the present XAFS analysis. On the other hand, XANES also shows that the valence changes to Ag^0; the intensity of the white line peak becomes smaller and the energy shifts to slightly higher as the samples are heat-treated both in atmosphere and in vacuum. These XANES behaviours indicate the existence of Ag clusters or a component of Ag^0 as discussed previously (Suzuki *et al.*, 2005). Although unfortunately we did not study X-ray diffraction (XRD), transmission electron microscopy and electron diffraction for the present Ag-zeolite samples, Altantzis *et al.* presented direct observations of Ag clusters using XRD and HAADF-STEM for the Ag zeolite-X as similarly heat-treated as in our present study (Altantzis *et al.*, 2016).

In Table 5, the local structure parameters for Ag—Ag interactions are summarized along with the PL emission energy. The interatomic distances for Ag clusters produced by heating are similar among the three zeolites, *i.e.* they are 2.82 ± 0.01 Å. On the other hand, the coordination number is different: N_{Ag} for Ag_{12}-A is 3.0 ± 0.3, N_{Ag} for Ag_{86}-X is 2.3 ± 0.3. The cluster models estimated from N_{Ag} are Ag_4 for Ag_{12}-A and Ag_3 for Ag_{86}-X.

Table 5
Interatomic distances (r_{Ag} ± 0.01 Å) and coordination numbers (N_{Ag} ± 0.3) for the Ag—Ag interaction for the unheated species, and for Ag clusters and cluster deformed species; the PL energy at 365 nm excitation is also listed.

	Interatomic distance / coordination number			
	Unheated	Ag clusters	Deformed	PL energy
Ag_{12}-A	2.87 Å / 1.3	2.81 Å / 3.0	2.87 Å / 1.2	2.18 eV
Ag_{86}-X	2.98 Å / 1.7	2.83 Å / 2.8	2.97 Å / 1.5	2.24 eV

As for Ag_{12}-A (Nakamura *et al.*, 2014), the Ag clusters are broken and the local structure around the Ag atoms returns to almost a similar state as for the unheated species by cooling to RT under air, existing also for Ag_{86}-X, but the local structure around the Ag atoms does not completely coincide with that for the unheated species. This result is supported by IR spectra where clear differences appear between the unheated species and after exposure to air (Fig. 6). The IR structure assigned to the framework of zeolite after heating and air exposure is different from that for the unheated species.

Ag_{12}-A and Ag_{86}-X show a strong enhancement of PL intensity by cooling with air after heating to ∼400°C, but no PL enhancement appears in the unheated species and heated species under the existence of Ag clusters (Nakamura *et al.*, 2014).

The Ag—Ag interatomic distances r_{Ag} after cooling with air (luminescent species, after full exposure to air) are 2.87 ± 0.01 Å for Ag_{12}-A and 2.98 ± 0.01 Å for Ag_{86}-X; it is interesting that these orders are the same as those of the packing ratio of the Ag atoms in the cavity (*i.e.* the number of Ag atoms to volume of unit cell, A > X). That is, highly packed species have contracted structures and show shorter Ag—Ag distances.

On the other hand, the energies of the PL are 2.18 eV for Ag_{12}-A and 2.24 eV for Ag_{86}-X excited by 365 nm laser [as shown in Fig. 1(*b*) and Table 5, which may correspond to the result that the lower the packing ratio, the higher the PL energy, as reported by De Cremer *et al.* (2009). The longer the Ag—Ag distance in the Ag zeolite species, the higher the PL emission energy.

We have discussed the local structure change around Ag atoms for Ag_{12}-A and Ag_{86}-X during heating (cluster formation process) and following cooling with air (cluster deformation process) by XAFS analyses. The structure model of Ag clusters is almost the same as that proposed previously. However, in the luminescent Ag zeolite species, Ag clusters no longer exist, and they are deformed to similar structures as the unheated species; whereas the local structure of deformed species is rather similar to that of the unheated species but confirmed to be different. At the present stage, we cannot

estimate the difference between them, but it should be a key point to reveal the luminescent species and the mechanism of this system.

5. Conclusion

We studied the *in situ* XAFS for the structural changes of Ag clusters in luminescent Ag_{12}-A and Ag_{86}-X produced by thermal treatment in atmosphere and in vacuum. It was confirmed that the Ag clusters were broken when the zeolite is exposed to air for Ag_{86}-X, which complement our previous results for Ag_{12}-A. After the air exposure, the strong PL still appears; it is suggested that the deformation of the Ag clusters plays an important role in the generation of the strong PL band and Ag clusters may not be direct species producing the strong PL. It is found that the local structure of Ag ions is slightly different (bond distances are slightly shorter) than for the unheated species which are induced by the formation and breakdown of Ag clusters; this is key point of the PL enhancement mechanism.

Acknowledgements

The synchrotron radiation experiments were performed at the Photon Factory in KEK under Proposals 2011G586, 2014G054 and 2016G056. The authors are greatly thankful to Dr D. Grandjean for fruitful discussions.

Funding information

This work was supported by JSPS KAKENHI Grant Numbers JP16K05011 and JP17K05026.

References

Altantzis, T., Coutino-Gonzalez, E., Baekelant, W., Martinez, G. T., Abakumov, A. M., Tendeloo, G. V., Roeffaers, M. B. J., Bals, S. & Hofkens, J. (2016). *ACS Nano*, **10**, 7604–7611.

Ankudinov, A. L., Ravel, B., Rehr, J. J. & Conradson, S. D. (1998). *Phys. Rev. B*, **58**, 7565–7576.

Calzaferri, G., Leiggener, C., Glaus, S., Schürch, D. & Kuge, K. (2003). *Chem. Soc. Rev.* **32**, 29–37.

Coutino-Gonzalez, E., Baekelant, W., Grandjean, D., Roeffaers, M. B. J., Fron, E., Aghakhani, M. S., Bovet, N., Van der Auweraer, M., Lievens, P., Vosch, T., Sels, B. & Hofkens, J. (2015). *J. Mater. Chem. C.* **3**, 11857–11867.

Coutino-Gonzalez, E., Grandjean, D., Roeffaers, M., Kvashnina, K., Fron, E., Dieu, B., De Cremer, G., Lievens, P., Sels, B. & Hofkens, J. (2014). *Chem. Commun.* **50**, 1350–1352.

Coutino-Gonzalez, E., Roeffaers, M. B. J., Dieu, B., De Cremer, G., Leyre, S., Hanselaer, P., Fyen, W., Sels, B. & Hofkens, J. (2013). *J. Phys. Chem. C*, **117**, 6998–7004.

De Cremer, G., Coutiño-Gonzalez, E., Roeffaers, M. B. J., De Vos, D. E., Hofkens, J., Vosch, T. & Sels, B. F. (2010). *ChemPhysChem*, **11**, 1627–1631.

De Cremer, G., Coutiño-Gonzalez, E., Roeffaers, M. B. J., Moens, B., Ollevier, J., Van der Auweraer, M., Schoonheydt, R., Jacobs, P. A., De Schryver, F. C., Hofkens, J., De Vos, D. E., Sels, D. F. & Vosch, T. (2009). *J. Am. Chem. Soc.* **131**, 3049–3056.

Fenwick, O., Coutiño-Gonzalez, E., Grandjean, D., Baekelant, W., Richard, F., Bonacchi, S., De Vos, D., Lievens, P., Roeffaers, M., Hofkens, J. & Samorì, P. (2016). *Nat. Mater.* **15**, 1017–1022.

Hoshino, H., Sannohe, Y., Suzuki, Y., Azuhata, T., Miyanaga, T., Yaginuma, K., Itoh, M., Shigeno, T., Osawa, Y. & Kimura, Y. (2008). *J. Phys. Soc. Jpn*, **77**, 064712–064717.

Kim, S. Y., Kim, Y. & Seff, K. (2003). *J. Phys. Chem. B*, **107**, 6938–6945.

Kim, Y. & Seff, K. (1987). *J. Phys. Chem.* **91**, 668–671.

Miyanaga, T., Suzuki, Y., Matsumoto, N., Narita, S., Ainai, T. & Hoshino, H. (2013). *Micropor. Mesopor. Mater.* **168**, 213–220.

Miyanaga, T., Suzuki, Y. & Narita, S. (2016). *Zeolites: Useful Minerals*, ch. 8, pp. 153–166. Intech.

Nakamura, A., Narita, M., Narita, S., Suzuki, Y. & Miyanaga, T. (2014). *J. Phys. Conf. Ser.* **502**, 012033.

Rodrigues, S. A. (1995). *Vib. Spectrosc.* **9**, 225–228.

Sakane, H., Miyanaga, T., Watanabe, I., Matsubayashi, N., Ikeda, S. & Yokoyama, Y. (1993). *Jpn. J. Appl. Phys.* **32**, 4641–4647.

Seifert, R., Rytz, R. & Calzaferri, G. (2000). *J. Phys. Chem. A*, **104**, 7473–7483.

Sun, T. & Seff, K. (1994). *Chem. Rev.* **94**, 857–870.

Suzuki, Y., Miyanaga, T., Hoshino, H., Matsumoto, N. & Ainai, T. (2005). *Phys. Scr.* T**115**, 765–768.